

Superconductivity in layered Zintl phase LiSn_2As_2

Junjie Wang^{†,1,2} Xiangru Cui^{†,1,2} Yimin Wan^{†,3} Tianping Ying^{*,1} Shiyao Li³ and Jiangang Guo^{*,1,2,4}

¹*Beijing National Laboratory for Condensed Matter Physics,*

Institute of Physics, Chinese Academy of Sciences, Beijing 100190, China

²*School of Physical Sciences, University of Chinese Academy of Sciences, Beijing 100049, China*

³*State Key Laboratory of Surface Physics, Department of Physics, Fudan University, Shanghai 200438, China*

⁴*Songshan Lake Materials Laboratory, Dongguan 523808, China*

(Dated: January 17, 2022)

We report the superconductivity in the layered Zintl phase LiSn_2As_2 , which is isostructural to NaSn_2As_2 and has a transition temperature (T_c) of 1.6 K. Despite similar T_c and Debye temperatures, substituting of Na with Li considerably increases the upper critical field. Based on a systematically comparison of Sn_4As_3 , NaSnAs , NaSn_2As_2 , $\text{Na}_{1-x}\text{Sn}_2\text{P}_2$, SrSn_2As_2 , and LiSn_2As_2 , we propose that carrier doping, intimately related to the formation of lone-pair electrons, controls superconductivity in layered SnAs-based compounds rather than chemical pressure. The current findings provide a thorough and comprehensive understanding of Sn-based Zintl phase.

I. INTRODUCTION

The Zintl phase is the product where alkali metal or alkaline earth reacts with any post-transition metals (Group 13 or 14) or p elements [1, 2]. There is usually a complete electron transfer from the more electropositive metal to anion clusters (Zintl ion), such as $(\text{Si}_4)^{4-}$ [3], $(\text{Te}_4)^{8-}$ [4] and $(\text{As}_7)^{3-}$ [5]. When the Zintl ion is composed of infinite 2D layers, these compounds are called layered Zintl phase with numerous features including superconductivity [6, 7], topological properties [8–11] and thermoelectricity [12, 13]. NaSn_2As_2 , with a superconducting transition temperature at 1.6 K, has recently attracted a lot of attention [6, 14]. Later research discovered that NaSn_2As_2 can be prepared into few layers by mechanical and liquid-phase exfoliation. Substitution of As for a smaller P will increase the T_c to 2 K [7], while SrSn_2As_2 is proved to be a 3D Dirac semimetal without superconductivity [15, 16]. Detailed investigation suggests the T_c enhancement in $\text{Na}_{1-x}\text{Sn}_2\text{P}_2$ is due to additional charge donation from Na vacancies. However, the positive chemical pressure generated by P with a small radius can not be neglected. By the same token, replacing Na with a greater Sr will result in a negative pressure, which is consistent with the absence of superconductivity in SrSn_2As_2 . As a result, the increase in T_c in the SnAs-based layered Zintl phase cannot be attributed solely to carrier doping or chemical pressure.

NaSnAs and NaSnP [17, 18], on the other hand, are two closely $\text{NaSn}_2\text{As}(\text{P})_2$ related compound by inserting one more Na ion in each $\text{SnAs}(\text{P})$ layer (Fig. 1(b)). Different from NaSn_2As_2 and $\text{Na}_{1-x}\text{Sn}_2\text{P}_2$ [7, 14], NaSnAs and NaSnP are indirect band gap semiconductors with narrow gaps of about 0.31 and 0.62 eV, respectively [12]. It is reported that $\text{NaSnAs}(\text{P})$ shows a much lower thermal conductivities than $\text{NaSn}_2\text{As}(\text{P})_2$ due to the surplus lone-pair electrons. The lone pair is defined as a pair of valence electrons that are not shared with another atom to form a covalent bond. Sn and As(P) are covalently

bonded to form a tetrahedron, as shown in Fig. 1(e). In the case of $\text{NaSnAs}(\text{P})$, with the one electron from Na, both Sn and As(P) enter a full outer shell structure, leaving two sets of lone-pair electrons dangling outside of the plane. SrSn_2As_2 follows the same logic, as Sr contributes two electrons to the system. Previous research found that surplus lone-pair electrons will generate strong in-harmonic vibration and increase the Gruneisen parameters [19–21]. To fully understand the dominant factor of superconductivity in the series of Sn-based layered Zintl phase, new compounds that may generate chemical pressure without introducing extra carrier doping are highly desired.

In this work, we report the discovery of a new compound LiSn_2As_2 that is isostructural to NaSn_2As_2 . Compared with NaSn_2As_2 , LiSn_2As_2 has a similar T_c at 1.6 K, but a much-enhanced upper critical field (H_c). First principle calculation reveals a significant change of the Fermi surface topology by the substitution of Li. Combined with experimental and theoretical analyses, we infer that the appearance of superconductivity in A-Sn-As system is dominated by the charge carrier doping, rather than chemical pressure. Finally, we provide a unified understanding towards the reported Sn-based layered Zintl phases, with NaSn_2Pn_2 serving as a parent phase for the series of superconductors.

II. EXPERIMENTS

Synthesis

Stoichiometric amount of Li, Sn, and As were mixed and loaded into an alumina crucible, sealed into an evacuated quartz tube. Heated to 925 K with duration of 20 hours. Then, the sintered sample was taken out, reground, pelletized and heated to 900 K for 20 hours for adequate distribution. The sample preparation process are handled in a glove-box filled with argon gas. LiSn_2As_2 single crystals can be grown by using Sn-flux

method, the sealed quartz tube was heated to 1200 K in 20 hours, slowly cooled to 1000 K with a rate of 3 K/h. The excess Sn is removed by centrifugation. Single crystal with size of $1.5 \times 1.5 \times 0.1 \text{ mm}^3$ can thus be obtained.

Characterization

Powder X-ray diffraction (XRD) data were collected using a PANalytical X'Pert PRO diffractometer (Cu $K\alpha$ -radiation) with a graphite monochromator in a reflection mode. Rietveld refinement of PXRD pattern was performed using Fullprof software suites [22]. The composition of Sn and As was determined by Energy Dispersive Spectroscopy (EDS), the elements ratio and element valence state information of Li, Sn and As were determined by inductively coupled plasma atomic emission spectroscopy and X-ray photoelectron spectroscopy (ICP-AES and XPS). Electrical resistivity and Hall resistivity were measured through standard six-wire method using the physical property measurement system (PPMS-9T, Quantum Design).

Theoretical calculation

First-principles calculations were carried out with the density functional theory (DFT) implemented in the Vienna ab initio simulation package (VASP) [23]. The generalized gradient approximation (GGA) in the form of Perdew-Burke-Ernzerhof (PBE) [24] was adopted for the exchange-correlation potentials. We used the projector augmented-wave (PAW) [25] pseudopotentials with a plane wave energy of 800 eV; $1s^2 2s^1$, $4d^{10} 5s^2 5p^2$ and $4s^2 4p^3$ were treated as valence electrons for Li, Sn and As, respectively. A Monkhorst-Pack Brillouin zone sampling grid with a resolution $0.02 \times 2\pi \text{ \AA}^{-1}$ was applied [26]. Atomic positions and lattice parameters were fully relaxed till all the forces on the ions were less than 10^{-4} eV/\AA . The lattice parameters after relaxation were $a = 4.03085 \text{ \AA}$ and $c = 25.85439 \text{ \AA}$, agreeing well with the experimental values within a deviation of 0.6%. This confirmed the reliability of the calculation. Phonon spectra were calculated on a $2 \times 2 \times 1$ supercell using the finite displacement method implemented in the PHONOPY code to determine the lattice dynamical stability of the structures [27]. The band structure of NaSn_2As_2 was calculated for comparison using the same parameter except for the cut off energy was set to be 400 eV.

III. RESULTS AND DISCUSSION

LiSn_2As_2 is a new compound, isostructural to the well-studied NaSn_2As_2 . Figure 1 depicts all of the known Sn-based Zintl phase, including Sn_4As_3 , NaSnAs and ASn_2Pn_2 ($A = \text{Li}/\text{Na}/\text{Sr}$, $\text{Pn} = \text{As}/\text{P}$), which crystallize in a space group of $R\bar{3}m$ (No.166) and can be viewed as different stacking sequence of the SnPn layers with Na or other guest species. As shown in Fig. 1(a), Sn_4As_3 has two types of Sn-As configurations [28]. In one build-

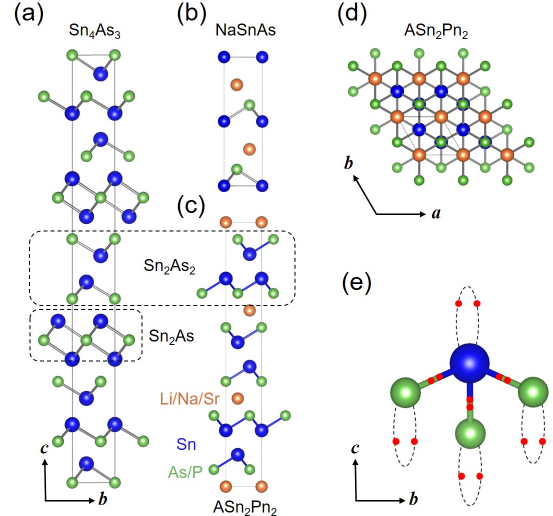


FIG. 1. (a-c) Crystal structures of Sn_4As_3 , NaSnP , ASn_2Pn_2 ($A = \text{Li}/\text{Na}/\text{Sr}$, $\text{Pn} = \text{As}/\text{P}$). (d) The crystal structure of ASn_2Pn_2 along the c -direction. (e) Schematic diagram of long-pair electrons in Sn-based compound systems.

ing block, each Sn (As) atom is coordinated by three As (Sn) atom to form a Sn_2As_2 layer, while the other Sn atom is joined to six As atoms to form a Sn_2As layer. As a result, Sn_4As_3 can be written as $(\text{Sn}_2\text{As})\text{Sn}_2\text{As}_2$ (Fig. 1(a)), NaSnAs (Fig. 1(b)) and NaSn_2Pn_2 (Figs. 1(c) and (d)) share a similar stacking sequence of SnPn and A layers with the variation of Na in each SnPn layer or every two layers along the c axis. Figure 1(e) is the schematic diagram of the local electronic configuration of the SnAs tetrahedra. The covalent bonds between Sn and As are composed of the p orbitals, while the dangling lone-pair electrons are contributed by the s^2 orbitals of Sn and As. For NaSnPn and SrSn_2As_2 , the lone-pair orbitals are fully occupied, while the lone-pair on the Sn side is proved to be partially occupied in NaSn_2As_2 .

Figure 2(a) shows the Rietveld refinements of powder diffraction pattern of LiSn_2As_2 , yielding the lattice constants $a = 4.0072(3) \text{ \AA}$ and $c = 25.7008(6) \text{ \AA}$. The refinement converged to the figures of merit $R_p = 5.32\%$, $R_{wp} = 7.36\%$ and $\chi^2 = 2.63$. The lattice change of the a and c axes are -0.02% and 6.82% , respectively, as compared to NaSn_2As_2 with $a = 4.006 \text{ \AA}$, $c = 27.581 \text{ \AA}$ [12], demonstrating the realization of chemical pressure. The diffraction pattern of a single crystal LiSn_2As_2 sample with $00l$ preferred orientation is shown in Fig. 2(b), and the optical image is shown in the inset. XPS and ICP measurements were used to validate the element ratio and valence states in LiSn_2As_2 . As the XPS spectra of Li $1s$ orbital shown in Fig. 2(c), the binding energy of Li $1s$ is 54.3 eV , consisting with that of Li^+ . This shows that the Li ion has entirely lost its out shell electron to $(\text{Sn}_2\text{As}_2)^-$. Besides, the peaks of Sn $3d^{3/2}$ and

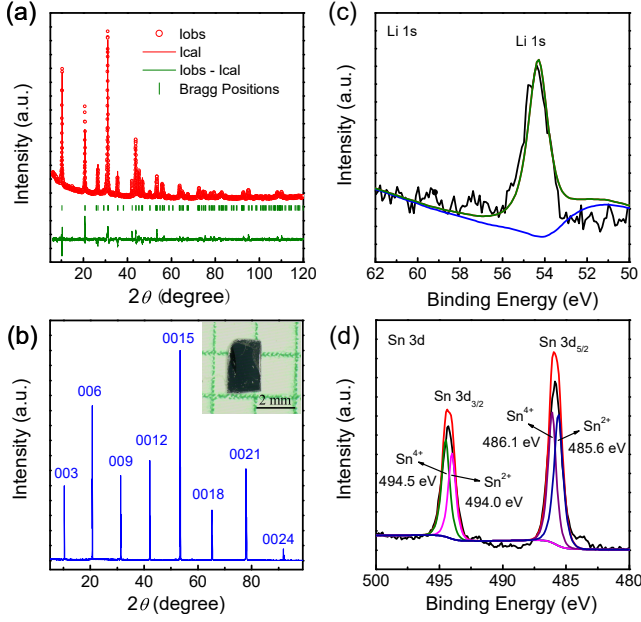


FIG. 2. (a) Rietveld refinements of powder x-ray diffraction (PXRD) pattern of LiSn_2As_2 at temperature at 300 K. (b) The XRD patterns of LiSn_2As_2 single crystal, where the preferred orientation of 00 l peaks can be seen. Inset shows the optical images of LiSn_2As_2 single crystal. (c, d) XPS spectrum of Li-1 s Sn-3 d orbit of LiSn_2As_2 .

$3d^{5/2}$ orbital locate at 494.3 eV and 485.9 eV, respectively (Fig. 2(d)), and both of them can be separated into Sn^{4+} and Sn^{2+} peaks. Meanwhile, the chemical formula of stoichiometric $\text{Li}:\text{Sn}:\text{As} = 1:2:2$ is determined by ICP. LiSn_2As_2 single crystal exhibits a metallic behavior from 2 to 300 K (Fig. 3(a)). The residual resistivity ratio (RRR) value is calculated to be 1.36, which is lower than that of NaSn_2As_2 at 3.7 [14]. To further comprehend its normal state behavior of LiSn_2As_2 , we use the Bloch-Gruneisen (BG) model to fit the resistance curve [29, 30]

$$\rho(T) = \rho_0 + 4R(\Theta_R) \left(\frac{T}{\Theta_R} \right)^z \int_0^{\Theta_R/T} \frac{x^z dx}{(e^x - 1)(1 - e^{-x})}$$

where T stands for temperature and Θ_R for Debye temperature. For electron-electron interaction, s - d electron scattering, and electron scattering by phonons, the value z could be 2, 3, or 5. The fitting curves of three alternative scattering mechanisms are shown in Figure 3(a). The raw data is best fitted by the curve with $z=5$. In the LiSn_2As_2 system, the phonon dominates the scattering of normal state resistance. Other fitting parameters are $\rho_0=0.499 \text{ m}\Omega\cdot\text{cm}$, $\rho(\Theta_R)=0.614 \text{ m}\Omega\cdot\text{cm}$ and $\Theta_R=194 \text{ K}$. To ensure that the BG fitting is correct, we measured the heat capacity of a single LiSn_2As_2 crystal, as shown in Fig. 3(b). The dotted line in Fig. 3(b) represents the Dulong-Petit limit, which is closed at $C_p(200 \text{ K})=118.64 \text{ J mol}^{-1} \text{ K}^{-1}$. The inset shows C_p/T as a function of T^2

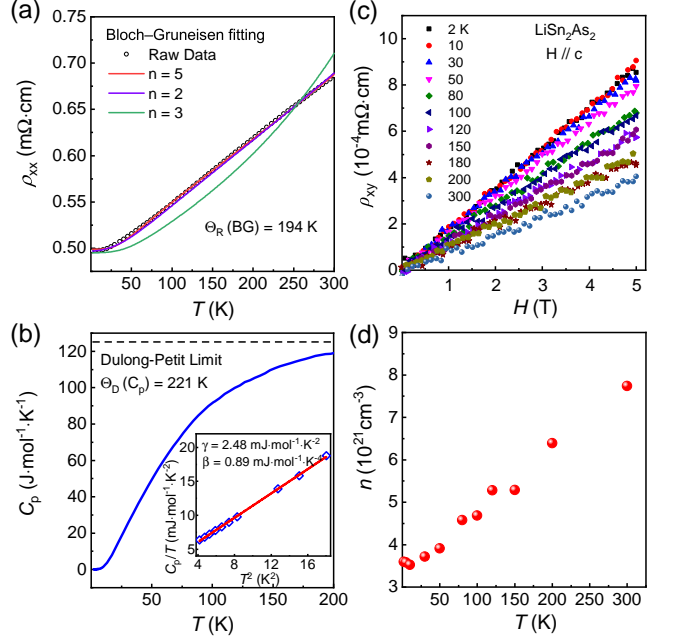


FIG. 3. (a) Resistivity of the LiSn_2As_2 single crystal from 2 to 300 K, the circles represent raw data and the solid lines are Bloch-Gruneisen fitting curve with $z=2,3$ and 5. (b) Specific heat (C_p) as a function of temperature of LiSn_2As_2 single crystal. Inset shows C_p/T as a function of T^2 from 2-5 K. (c) Hall resistance of LiSn_2As_2 single crystal with $H//c$ axis. (d) Carrier concentrations of LiSn_2As_2 single crystal as a function of temperature.

in the temperature range of 2-5 K. The fitting formula is [31]

$$\frac{C_p}{T} = \gamma + \beta T^2$$

$$\Theta_D = \sqrt[3]{\frac{12\pi^4 N_A k_B}{5\beta}}$$

where γ is the electronic specific heat coefficient and β refers to the phonon specific heat coefficient. The fitted parameters are $\gamma=2.48 \text{ mJ mol}^{-1} \text{ K}^{-2}$, $\beta=0.89 \text{ mJ mol}^{-1} \text{ K}^{-2}$ and $\Theta_D=221 \text{ K}$, which is close to the value obtained by BG model. The Debye temperature of LiSn_2As_2 is comparable to that of NaSn_2As_2 ($\Theta_D=205 \text{ K}$) and SrSn_2P_2 ($\Theta_D=237 \text{ K}$). The Hall resistance and extracted carrier density of LiSn_2As_2 are shown in Figs. 3(c) and (d). The positive slope and linear behavior of Hall resistance indicate that LiSn_2As_2 is a single band p-type metal. The carrier density (n) is calculated by the single band model

$$n = \frac{1}{eR_H}$$

where e is elementary charge and R_H refers to Hall coefficient. The carrier concentration of LiSn_2As_2 is 3.59×10^{21}

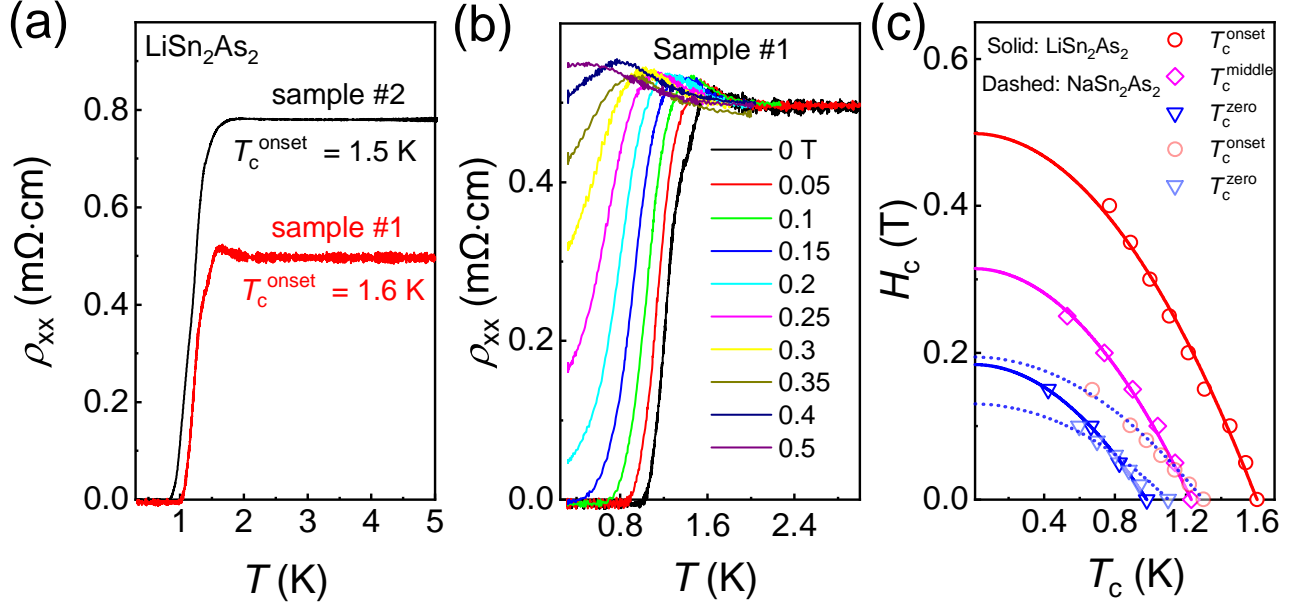


FIG. 4. (a) Low-temperature resistivity of two LiSn_2As_2 single crystals from 0.3 to 5 K. (b) Low-temperature resistivity at different magnetic fields parallel to the c axis. (c) The upper critical fields ($H_c(0)$) fitted by T_c^{onset} , T_c^{middle} and T_c^{zero} with $H//c$ axis. The dashed curve are the $H_{c2}(T)$ of NaSn_2As_2 extracted from Ref [6]

cm^{-3} at 2 K and $7.74 \times 10^{21} \text{ cm}^{-3}$ at 300 K, confirming the metallic nature.

Because LiSn_2As_2 and NaSn_2As_2 have similar transport behavior and Debye temperatures, we are interested in learning more about LiSn_2As_2 's ultra-low temperature behavior. The resistivity of two batches of LiSn_2As_2 single crystals in the temperature range of 0.3-5 K is shown in Fig. 4(a). A sharp decline in resistivity can be seen at 1.6 K, with a zero resistance reaching at 1 K. There are slight differences between two batches of LiSn_2As_2 single crystals. The sample with lower residual resistance (#2) shows a lightly lower $T_c^{\text{onset}} = 1.5$ K than that of sample #1, implying the small variation of T_c is caused by sample quality. The suppression of superconductivity at various external magnetic fields is seen in Fig. 4(b). In the presence of a magnetic field, the sample exhibits a tiny hump. This hump can also be seen in other instances, such as NdCeCuO and BiSrCaCuO [32, 33], which is generally considered to be the result of imperfection of the single crystals. Figure 4(c) shows the upper critical fields $H_c(0)$ fitted by Ginzburg-landau equation

$$H_c(T) = H_c(0) \left[1 - \left(\frac{T}{T_c} \right)^2 \right]$$

The fitted $H_c(0)$ are 0.49 T, 0.31 T and 0.18 T for T_c^{onset} , T_c^{middle} and T_c^{zero} , respectively. We note that the acquired $H_c(0)$ of LiSn_2As_2 is much higher than that of NaSn_2As_2 (0.31 T for T_c^{onset} and 0.15 T for T_c^{zero} , superimposed as dotted lines in Fig. 4(c)).

Figure 5(a) depicts the initial Brillouin zone and the

rhombohedral lattice's high symmetry route. The corresponding band structure and partial density of states (PDOS) are shown in Fig. 5(b). The bands of LiSn_2As_2 are more electron doped than the band structure of NaSn_2As_2 (shown as a dash curve), which is consistent with our Hall measurement. Furthermore, the Sn- s , Sn- p , and As- p orbitals are mainly responsible for the bands around the fermi level (E_F). The s orbital of Sn, in particular, contributes 18.3% of the total DOS at the E_F , whereas the s orbital of As lies -10 eV below the E_F (not shown here). LiSn_2As_2 has two sets of Fermi surface (shown in Fig. 5(c)), the cylindrical shape one is similar to that of NaSn_2As_2 [34], while the bowl shape one around Z point is attributed to the local hole-doped band characteristic of LiSn_2As_2 , as the corresponding band in NaSn_2As_2 is located just below the Fermi level around Z point. The stability of the acquired LiSn_2As_2 is substantiated by the phonon calculations presented in Fig. 5(d). A neglectable imaginary frequency around Γ is caused by numerical noise.

Finally, we discuss the superconducting control parameter in the Sn-based layered Zintl phase. The volume contraction of 6.75% indicates that the iso-electron substitution of Na by Li produces an effective positive chemical pressure in NaSn_2As_2 . The observation of superconductivity in LiSn_2As_2 and the comparable T_c rule out chemical pressure as a key driver in T_c increase. Meanwhile, NaSnAs and NaSnP are semiconductors with narrow band gaps at about 0.31 eV and 0.63 eV respectively, and SrSn_2As_2 is a semimetal [15, 35]. This semiconducting or semimetallic behavior can be explained in terms of

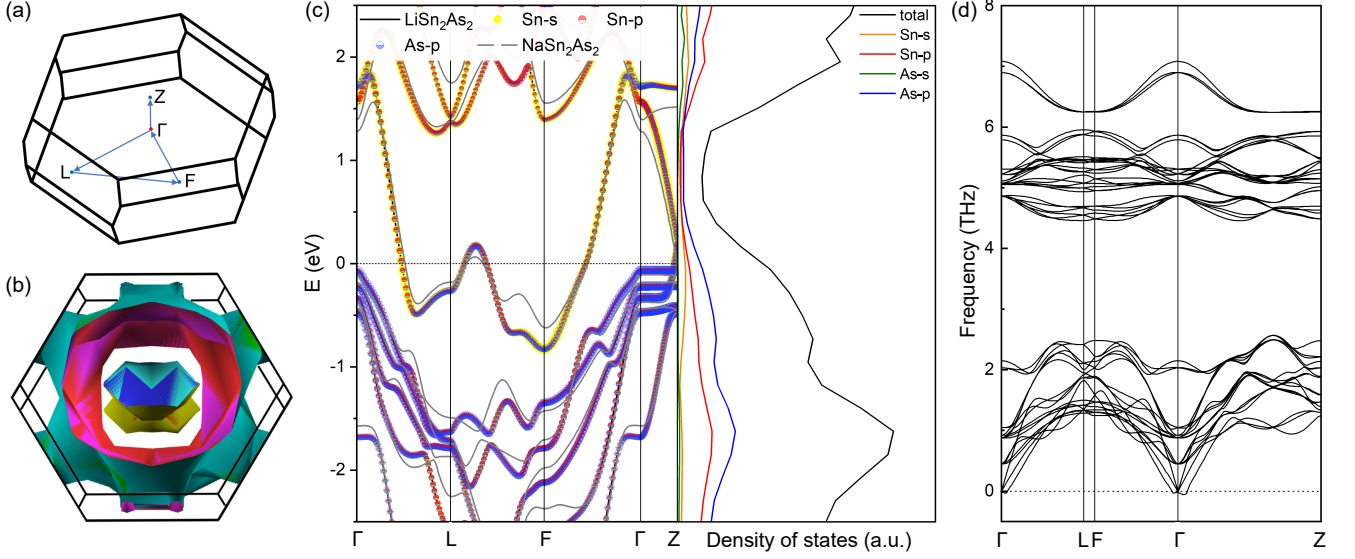


FIG. 5. (a) First Brillouin zone and the high symmetry K-path of LiSn₂As₂. The Fermi surface (b), band structure and partial density of states (PDOS) (c) and phonon spectrum (d) of LiSn₂As₂. The bands of NaSn₂As₂ are superimposed in Fig. 5(c) as gray curve for comparison.

lone pair electrons, where the Sn-Pn tetrahedra have saturated electron pairs and the ionic bonds between the alkali metal Na and the Zintl ion SnPn do not have enough itinerant electrons, as briefly discussed in the introduction. Any hole doping can effectively tip the charge balance and boost conductivity in these double lone pair electrons, which serve as a charge reservoir. This is exactly the case of superconducting NaSn₂As₂, LiSn₂As₂ and Na_{1-x}Sn₂P₂ by partial removal of electrons from the lone pair electrons. This observation is consistent with our Hall results of p -type charge carrier, and NaSnAs can be considered as a parent phase of the Sn-based layered Zintl phase. We infer that the (Sn₂As) slab in Sn₄As₃ provides less than one electron to the (SnAs) slab from this perspective. Because As or P have a stronger electronegativity than Sn, the charge transfer should take place on the Sn side, with the lone pair on the P side acting as a bridge of the charge transfer. Furthermore, the phonon vibration modes will be influenced by the quantity of lone pair electrons, which will affect the electron-phonon interaction and alter T_c . This could explain the slightly different T_c within NaSn₂As₂, Na_{1-x}Sn₂P₂ and LiSn₂As₂ (the slightly electron doping effect can be observed in Fig. 5(b)). Following this route, more exciting discovery can be anticipated. In SrSn₂As₂, for example, superconductivity may be achieved in a 3D Dirac semimetal by removing the electrons from the lone pair electrons through selective removal of Sr or substitution.

IV. CONCLUSION

In conclusion, we report the crystal structure, transport properties, heat capacity and electronic structure of LiSn₂As₂. In the range of 2-300 K, LiSn₂As₂ exhibits metallic behavior. The Θ_D obtained by BG model and Debye model are 194 K and 221 K, respectively, which is closed to that of NaSn₂As₂. Ultra-low temperature transport measurements reveals that LiSn₂As₂ is a superconductor with T_c^{onset} at 1.6 K. The upper critical field of LiSn₂As₂ is $H_c=0.49$ T, doubling that of NaSn₂As₂. We discovered that the amount of lone-pair electron acts as a charge reservoir and governs superconductivity by systematically analyzing the crystal structure and physical properties of Sn₄As₃, NaSnAs, NaSnP and ASn₂Pn₂. We anticipate similar phenomena can be realized in other layered Zintl phases.

ACKNOWLEDGMENTS

This work is financially supported by the National Key Research and Development Program of China (No. 2018YFE0202601 and 2017YFA0304700), the National Natural Science Foundation of China (No. 51922105 and 51772322), Beijing Natural Science Foundation (Grant No. Z2000005).

[†] These authors contribute equally

T.Y.: ying@iphy.ac.cn

J.G.: jgguo@iphy.ac.cn

-
- [1] HW Kohlschutter, “Theory and research - Eduard Zintl,” *NATURWISSENSCHAFTEN* **29**, 241–244 (1941).
- [2] F Laves, “Eduard Zintl’s work on chemistry and structure of alloys,” *NATURWISSENSCHAFTEN* **29**, 244–255 (1941).
- [3] Jialing Wang, Sabyasachi Sen, Ping Yu, Nigel D. Brown, and Susan M. Kauzlarich, “Synthesis and spectroscopic characterization of P-doped Na_4Si_4 ,” *JOURNAL OF SOLID STATE CHEMISTRY* **183**, 2522–2527 (2010).
- [4] Frank Albert Cotton, Geoffrey Wilkinson, Carlos A Murillo, Manfred Bochmann, and Russell Grimes, *Advanced inorganic chemistry*, Vol. 6 (Wiley New York, 1988).
- [5] Hua He, Chauntae Tyson, and Svilen Bobev, “New compounds with $[\text{As}_7]^{3-}$ clusters: Synthesis and crystal structures of the zintl phases Cs_2NaAs_7 , $\text{Cs}_4\text{ZnAs}_{14}$ and $\text{Cs}_4\text{CdAs}_{14}$,” *Crystals* **1**, 87–98 (2011).
- [6] Yosuke Goto, Akira Yamada, Tatsuma D Matsuda, Yuji Aoki, and Yoshikazu Mizuguchi, “SnAs-based layered superconductor NaSn_2As_2 ,” *Journal of the Physical Society of Japan* **86**, 123701 (2017).
- [7] Yosuke Goto, Akira Miura, Chikako Moriyoshi, Yoshihiro Kuroiwa, Tatsuma D Matsuda, Yuji Aoki, and Yoshikazu Mizuguchi, “ $\text{Na}_{1-x}\text{Sn}_2\text{P}_2$ as a new member of van der waals-type layered tin pnictide superconductors,” *Scientific reports* **8**, 1–8 (2018).
- [8] Lin-Lin Wang, Adam Kaminski, Paul C. Canfield, and Duane D. Johnson, “Different topological quantum states in ternary zintl compounds: BaCaX ($x = \text{si, ge, sn}$ and pb),” *The Journal of Physical Chemistry C* **122**, 705–713 (2018), <https://doi.org/10.1021/acs.jpcc.7b11111>.
- [9] Michael O. Ogunbunmi, Sviatoslav Baranets, Amanda B. Childs, and Svilen Bobev, “The Zintl phases AlIn_2As_2 ($A = \text{Ca, Sr, Ba}$): new topological insulators and thermoelectric material candidates,” *DALTON TRANSACTIONS* **50**, 9173–9184 (2021).
- [10] L. Y. Rong, J. Z. Ma, S. M. Nie, Z. P. Lin, Z. L. Li, B. B. Fu, L. Y. Kong, X. Z. Zhang, Y. B. Huang, H. M. Weng, T. Qian, H. Ding, and R. Z. Tai, “Electronic structure of SrSn_2As_2 near the topological critical point,” *SCIENTIFIC REPORTS* **7** (2017), 10.1038/s41598-017-05386-x.
- [11] Yuanfeng Xu, Zhida Song, Zhijun Wang, Hongming Weng, and Xi Dai, “Higher-order topology of the axion insulator EuIn_2As_2 ,” *Phys. Rev. Lett.* **122**, 256402 (2019).
- [12] Zhiping Lin, Gang Wang, Congcong Le, Huaizhou Zhao, Ning Liu, Jiangping Hu, Liwei Guo, and Xiaolong Chen, “Thermal conductivities in NaSnAs , NaSnP , and NaSn_2As_2 : Effect of double lone-pair electrons,” *Phys. Rev. B* **95**, 165201 (2017).
- [13] Shao-Fei Wang, Zhi-Gang Zhang, Bao-Tian Wang, Jun-Rong Zhang, and Fang-Wei Wang, “Zintl phase BaAgSb : Low thermal conductivity and high performance thermoelectric material in ab initio calculation,” *Chinese Physics Letters* **38**, 046301 (2021).
- [14] EJ Cheng, JM Ni, FQ Meng, TP Ying, BL Pan, YY Huang, Darren C Peets, QH Zhang, and SY Li, “Nodeless superconductivity in the SnAs-based van der waals-type superconductor NaSn_2As_2 ,” *EPL (Europhysics Letters)* **123**, 47004 (2018).
- [15] Q. D. Gibson, L. M. Schoop, L. Muechler, L. S. Xie, M. Hirschberger, N. P. Ong, R. Car, and R. J. Cava, “Three-dimensional dirac semimetals: Design principles and predictions of new materials,” *Phys. Rev. B* **91**, 205128 (2015).
- [16] Keisuke Shinozaki, Yosuke Goto, Kazuhisa Hoshi, Ryosuke Kiyama, Naoto Nakamura, Akira Miura, Chikako Moriyoshi, Yoshihiro Kuroiwa, Hidetomo Usui, and Yoshikazu Mizuguchi, “Thermoelectric Properties of the As/P-Based Zintl Compounds $\text{EuIn}_2\text{As}_{2-x}\text{P}_x$ ($x=0-2$) and SrSn_2As_2 ,” *ACS APPLIED ENERGY MATERIALS* **4**, 5155–5164 (2021).
- [17] Andrew M. Ochs, Prashun Gorai, Yaxian Wang, Michael R. Scudder, Karl Koster, Curtis E. Moore, Vladan Stevanovic, Joseph P. Heremans, Wolfgang Windl, Eric S. Toberer, and Joshua E. Goldberger, “Computationally Guided Discovery of Axis-Dependent Conduction Polarity in NaSnAs Crystals,” *CHEMISTRY OF MATERIALS* **33**, 946–951 (2021).
- [18] B. Eisenmann and U. Rößler, “Crystal structure of sodium phosphidostaimate(ii), NaSnP ,” *Zeitschrift für Kristallographie - New Crystal Structures* **213**, 28–28 (1998).
- [19] Marc Kastner, David Adler, and H. Fritzsche, “Valence-alternation model for localized gap states in lone-pair semiconductors,” *Phys. Rev. Lett.* **37**, 1504–1507 (1976).
- [20] R.J. Angel, “Dove, M.T. Structure and Dynamics an Atomic View of Materials.: Oxford (Oxford University Press), 2003. 356 pp. Price £49.95. ISBN 0-19-850677-5.” *Mineralogical Magazine* **67**, 827–828 (2003), <https://pubs.geoscienceworld.org/minmag/article-pdf/67/4/827/2915715/gsmminmag.67.4.19-boo.pdf>.
- [21] Li-Dong Zhao, Shih-Han Lo, Yongsheng Zhang, Hui Sun, Gangjian Tan, Ctirad Uher, C Wolverton, Vinayak P Dravid, and Mercouri G Kanatzidis, “Ultralow thermal conductivity and high thermoelectric figure of merit in SnSe crystals,” *Nature* **508**, 373–377 (2014).
- [22] Juan Rodríguez-Carvajal, “Recent advances in magnetic structure determination by neutron powder diffraction,” *Physica B: Condensed Matter* **192**, 55–69 (1993).
- [23] G. Kresse and J. Furthmüller, “Efficiency of ab-initio total energy calculations for metals and semiconductors using a plane-wave basis set,” *Computational Materials Science* **6**, 15–50 (1996).
- [24] John P. Perdew, Kieron Burke, and Matthias Ernzerhof, “Generalized gradient approximation made simple,” *Phys. Rev. Lett.* **77**, 3865–3868 (1996).
- [25] G. Kresse and D. Joubert, “From ultrasoft pseudopotentials to the projector augmented-wave method,” *Phys. Rev. B* **59**, 1758–1775 (1999).
- [26] Hendrik J. Monkhorst and James D. Pack, “Special points for brillouin-zone integrations,” *Phys. Rev. B* **13**, 5188–5192 (1976).
- [27] Atsushi Togo and Isao Tanaka, “First principles phonon calculations in materials science,” *Scripta Materialia* **108**, 1–5 (2015).
- [28] C A Marques, M J Neat, C M Yim, M D Watson, L C Rhodes, C Heil, K S Pervakov, V A Vlasenko, V M Pudalov, A V Muratov, T K Kim, and P Wahl, “Electronic structure and superconductivity of the non-centrosymmetric Sn_4As_3 ,” *New Journal of Physics* **22**, 063049 (2020).

- [29] Nevill Francis Mott, Howard Jones, H Jones, and Huw Jones, The theory of the properties of metals and alloys (Courier Dover Publications, 1958).
- [30] John Bardeen and David Pines, “Electron-phonon interaction in metals,” *Physical Review* **99**, 1140 (1955).
- [31] Michael Tinkham, Introduction to superconductivity (Courier Corporation, 2004).
- [32] M. A. Crusellas, J. Fontcuberta, and S. Piñol, “Giant resistive peak close to the superconducting transition in $\text{La}_{2-x}\text{Ce}_x\text{CuO}_4$ single crystals,” *Phys. Rev. B* **46**, 14089–14094 (1992).
- [33] Y. M. Wan, S. E. Hebboul, D. C. Harris, and J. C. Garland, “Interlayer josephson coupling of thermally excited vortices in $\text{Bi}_2\text{Sr}_2\text{CaCu}_2\text{O}_{8-y}$,” *Phys. Rev. Lett.* **71**, 157–160 (1993).
- [34] K. Ishihara, T. Takenaka, Y. Miao, O. Tanaka, Y. Mizukami, H. Usui, K. Kuroki, M. Konczykowski, Y. Goto, Y. Mizuguchi, and T. Shibauchi, “Evidence for *s*-wave pairing with atomic scale disorder in the van der waals superconductor NaSn_2As_2 ,” *Phys. Rev. B* **98**, 020503 (2018).
- [35] Zhiping Lin, Gang Wang, Congcong Le, Huaizhou Zhao, Ning Liu, Jiangping Hu, Liwei Guo, and Xiaolong Chen, “Thermal conductivities in NaSnAs , NaSnP , and NaSn_2As_2 : Effect of double lone-pair electrons,” *PHYSICAL REVIEW B* **95** (2017), 10.1103/PhysRevB.95.165201.